Available online at www.sciencedirect.com
SCIENCE DIRECT®
ELSEVIER
Photonics and Nanostructures – Fundamentals and Applications xxx (2004) xxx–xxx
PHOTONICS AND NANOSTRUCTURES Fundamentals and Applications
www.elsevier.com/locate/photonics

Positioning photonic crystal cavities to single InAs quantum dots

K. Hennessy[a,*], A. Badolato[a], P.M. Petroff[a,b], E. Hu[a,b]

[a]*Department of Electrical and Computer Engineering, University of California Santa Barbara, Santa Barbara, CA 93106, USA*
[b]*Materials Department, University of California, Santa Barbara, CA 93106, USA*

Received 2 June 2004; received in revised form 3 July 2004; accepted 5 July 2004

Abstract

We have investigated the optical properties of planar photonic crystal cavities formed by removing a single hole from a two-dimensional square lattice of air holes etched through a thin GaAs slab. We have demonstrated cavity resonances with quality factors (Q's) as high as 8500, using an internal light source provided by an ensemble of InAs quantum dots (QDs) grown by molecular beam epitaxy (MBE). The high-Q modes are confined to a very small mode volume, $V = 0.7(\lambda/n)^3$, making them attractive to study in the context of cavity quantum electrodynamics with single QDs, where a high $Q/\sqrt{V}$ is needed to observe the strong coupling between an electronic state of the dot and the optical cavity mode. To this end, we have developed an accurate and robust alignment technique that positions a photonic crystal cavity to a single QD with 25 nm resolution. We present the details of this new technology and demonstrate its effectiveness by strategically positioning a number of QDs within photonic crystal cavities at points where the electric field intensity is high.

PACS: 85.40.Ux; 85.60.-q

Keywords: Photonic crystal; Microcavity; Quantum dot; Coupling; Positioning

1. Introduction

Semiconductor quantum dots (QDs) are potentially useful elements for quantum information processing [1]. Many applications in this field, such as single-photon sources and quantum bits, can be achieved by positioning a single QD in an optical cavity that supports simultaneously high quality factor (Q) and small volume (V) electromagnetic modes. Maximizing the ratio Q/V of these modes increases the interaction of excitons captured in the QD with the electromagnetic field confined in the cavity. Interesting effects of this interaction include an increase in the spontaneous emission rate of the exciton by a factor proportional to Q/V, and, if $Q/\sqrt{V}$ is high enough, a

* Corresponding author. Tel.: +1 805 893 8012; fax: +1 805 893 6132.
E-mail address: kjh@ece.ucsb.edu (K. Hennessy).

1569-4410/$ – see front matter © 2004 Elsevier B.V. All rights reserved.
doi:10.1016/j.photonics.2004.07.001

coherent coupling of the exciton and photon states in a regime referred to as strong coupling.

Air-clad, planar photonic crystal defect cavities [2] are particularly interesting to study for these high *Q/V* applications since they can support defect modes with volumes approaching the theoretically smallest possible in a dielectric cavity. Our first characterization of ultra-small *V* cavities, based on a triangular lattice [3], revealed low *Q*'s, raising the question of whether a high *Q/V* could be demonstrated in this class of cavities. More recently, several ingenious, complimentary techniques to minimize vertical radiation loss from planar photonic crystal cavities have yielded a number of high-*Q* cavity designs [4–8]. Cavities based on these designs have been fabricated and demonstrated experimentally to possess very high-*Q*'s [7,9–11], showing quite convincingly that planar photonic crystal cavities are very well suited for high *Q/V* applications.

Natural emitters to embed in these cavities are self-assembled semiconductor QDs grown monolithically within the photonic crystal slab by molecular beam epitaxy (MBE). Several experiments have already observed emission from an ensemble of InAs QDs in photonic crystal cavities [9,11–13]. In these experiments, the QDs are distributed randomly throughout the cavity, at a high density ($>10^{10}$ cm^{-2}) to ensure that several dots possess both the correct position in the cavity and emission energy to couple with a cavity mode. To construct single-QD devices, one may rely on this random positioning approach in material with a much lower density of QDs, so that on the average only one dot is present in any cavity. However, in this case the probability of achieving coupling can become very small considering the extremely small *V*'s of defect modes. An attractive alternative to achieve coupling with a single dot is to actively position a QD in the cavity. Such an approach, although technically difficult, would be incredibly useful in the construction of single-QD devices and would offer a level of reproducibility not available using random positioning techniques. The primary focus of this work is to present a robust technique for actively positioning single QDs in photonic crystal cavities. Though well suited for positioning optical cavities of very small *V*, this technique can be used to align QDs to a variety of optical or electrical devices.

2. Cavity design

Various design concepts have been developed to boost the *Q* of specific planar photonic crystal defect modes. Loss reduction can be achieved through various design concepts such as Gaussian confinement [7], symmetry analysis [5], balancing the positive and negative field contributions in the mode [4], and recycling of the mirror losses through radiation modes [8]. Many of the cavity designs inspired by these concepts rely on a non-trivial shrinking/shifting of the photonic crystal holes near the defect, as compared to the bulk crystal. While this has proven to increase the *Q* of the cavity, it can also render devices very challenging to fabricate. Small or shifted holes represent a fabrication challenge since dry etch rates are always limited by the smallest hole and mask resiliency by the smallest distance between two holes. Thus, from a fabrication perspective, a cavity based on photonic crystal holes of uniform diameter and spacing would be ideal. Rather surprisingly, by simply removing a single hole from a square-lattice photonic crystal, one can create a defect cavity that is both relatively simple to fabricate and high *Q/V* [6]. A scanning electron micrograph (SEM) of this cavity geometry, referred to as the S1 cavity, is shown in Fig. 1 for a GaAs cavity with a ratio of hole radius to lattice constant of $r/a = 0.38$, $a = 290$ nm, and slab thickness $d = 175$ nm. Fine-tuning of the holes nearest to the defect is not necessary—this simple defect geometry supports a mode that is low-loss in the vertical direction, due to the inherent odd-symmetry of its component fields. The electric field intensity of this lowest-order, whispering gallery-like mode (WGM) is plotted in Fig. 2. From this intensity profile, it is apparent this mode is very well confined in the plane of the photonic crystal, a fact confirmed by our calculation of a small mode volume $V = 0.7(\lambda/n)^3$, using 3D FDTD software [14] for a device with $n = 3.54$. We now consider this device for coupling to a single QD. Although this defect is donor-like, the electric field intensity is not simply confined in the high-index region of the device. This mode has been classified as whispering-gallery like because the field intensity is highest at the perimeter of the defect, very near the first layer of photonic crystal holes. This presents a problem in light of recent experiments [15] revealing that positioning QDs < 40 nm from an air surface results in severe linewidth broadening, discounting placement of the QD

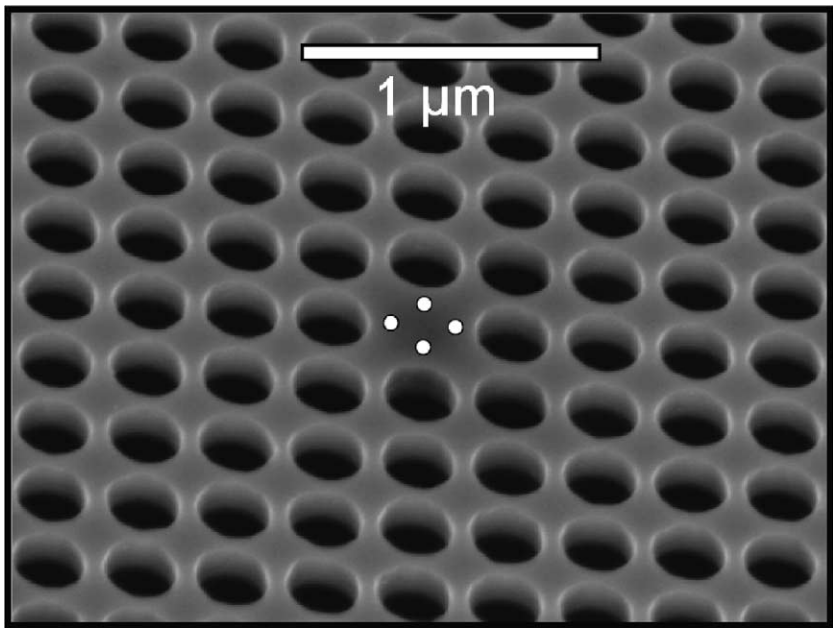

Fig. 1. Scanning electron micrograph of a single-hole defect, square-lattice photonic crystal cavity fabricated in GaAs. The lattice constant is 290 nm and the slab thickness is 175 nm. Desirable locations to place a single QD are indicated by filled white circles.

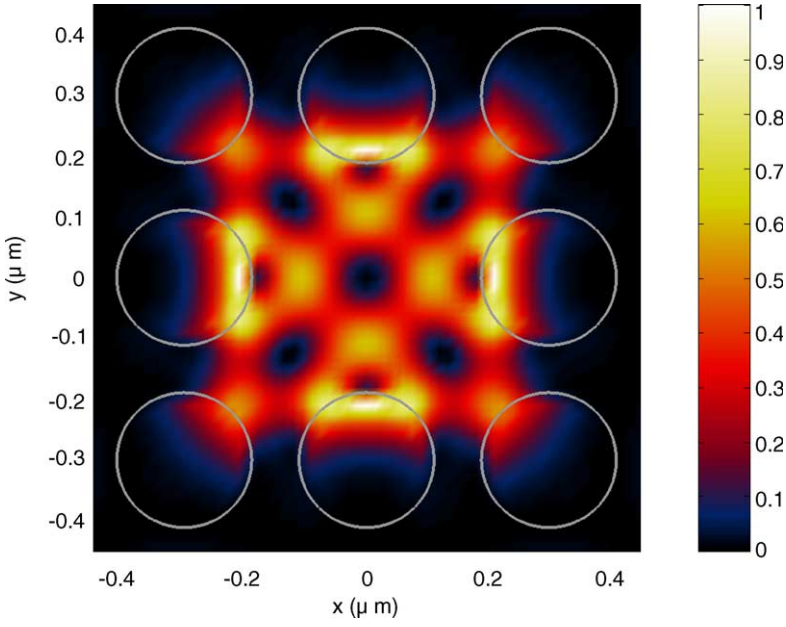

Fig. 2. Electric field intensity of the whispering-gallery-like mode in the S1 cavity, taken at the middle of the photonic crystal slab.

near any photonic crystal holes. However, four equivalent regions of high field exist closer to the center of the defect, ∼70 nm from any photonic crystal hole. At these locations, the field intensity reaches about 2/3 of the maximum value for this mode, and we conclude these are promising locations to place an individual QD. These desired placement points are indicated in Fig. 1 by filled white circles. Despite being restricted to placing a QD at a region of reduced intensity, the extremely high *Q/V* of this cavity should allow us to observe significant coupling with a single dot.

3. Device fabrication and characterization

To characterize the modal signature and *Q*'s of the S1 cavity, we use an active region consisting of five layers of InAs QDs, spaced by 30 nm, embedded in a GaAs slab of thickness $d = 175$ nm. Each layer of dots has a density of $\sim 2 \times 10^{10}$ cm^{-3}. This slab is grown on a 0.5 μm $Al_{0.7}Ga_{0.3}As$ layer that will be selectively removed to clad the entire cavity in air, providing strong vertical optical confinement. The photonic crystal pattern is defined in 4600 Å of ZEP 520A electron-beam resist with a 50 kV JEOL JBX-5DII (U) electron-beam lithography system. To ensure uniform hole diameter throughout the device, we apply a precise proximity effect correction to the cavity pattern as explained in [12,16]. A Panasonic E640 ICP etching system transfers the photonic crystal pattern directly from the ZEP resist into the (Al) GaAs heterostructure using a plasma generated from a gas mixture primarily composed of Ar and incorporating both Cl_2 and BCl_3. The optimal conditions for etching through an 180 nm GaAs slab are: 12 sccm Ar, 3 sccm BCl_3, 4 sccm Cl_2, 80 W bias power, 700 W ICP power, and 2.4 mTorr for 135 s. By flowing H_2O:HF (5:1) in the holes, we selectively etch the underlying $Al_{0.7}Ga_{0.3}As$ sacrificial layer for 30 s to release the final membrane structure. An example of our fabrication is shown in Fig. 1, where four of ten total lattice periods surrounding the defect are shown. Similar devices have been fabricated with a range of *a* from 280 to 320 nm and *r/a* from 0.36 to 0.40.

We use an internal light source with a continuous emission spectrum from 870 to 970 nm, provided by the embedded QDs, to decorate the cavity modes of our S1 structures. The sample is mounted in a He-flow cryostat and held at a constant temperature of 5 K. We then excite the QDs in the vicinity of a single defect with a diode laser operating in CW at 780 nm. We

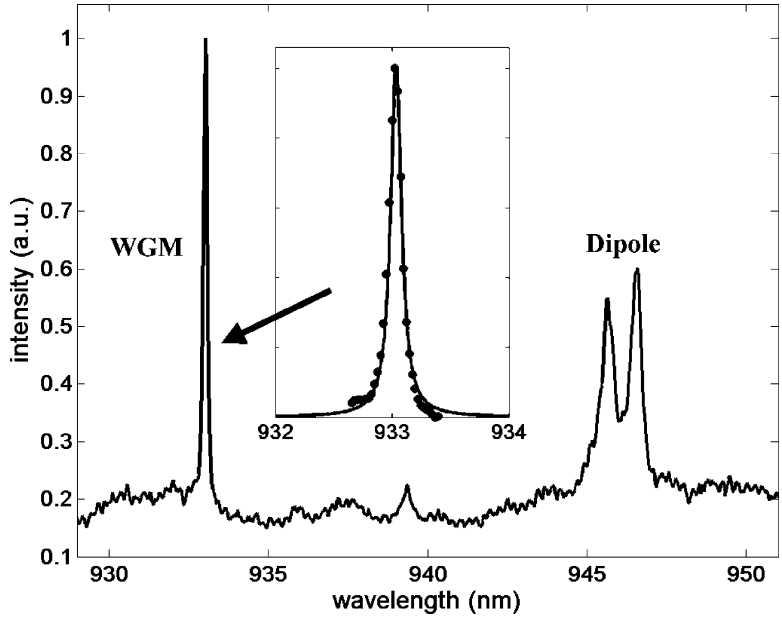

Fig. 3. Photoluminescence spectrum of an ensemble of InAs QDs embedded in an S1 cavity. The high-*Q* WGM is resonant at 933 nm and has been fit to a Lorentzian function with $Q = 8500$ in the inset. The lower-*Q*, doubly degenerate dipole mode is observed at longer wavelengths.

focus 1.8 kW/cm^2 power density on the sample surface at normal incidence in an estimated 3 μm spot size with a microscope objective (NA = 0.55) and collect the photoluminescence from the QD ensemble through the same objective. The QD emission is dispersed through a monochromator with 70 μeV resolution. Resulting spectra from the cavities, such as shown in Fig. 3, reveal a single high-Q mode 15–25 nm blue-shifted from a doubly-degenerate mode with a significantly lower Q. We attribute these peaks to the WGM and doubly degenerate dipole mode that are predicted to exist in this cavity. In the inset of Fig. 3, we have fit the peak corresponding to the WGM to a Lorentzian function with Q = 8500. The resonance wavelength of the WGM can be tuned over the entire QD ensemble spectrum by changing a, r/a, and the electron dose deposited in the photonic crystal holes during the electron-beam lithography [11]. The Q remains high over this wavelength range.

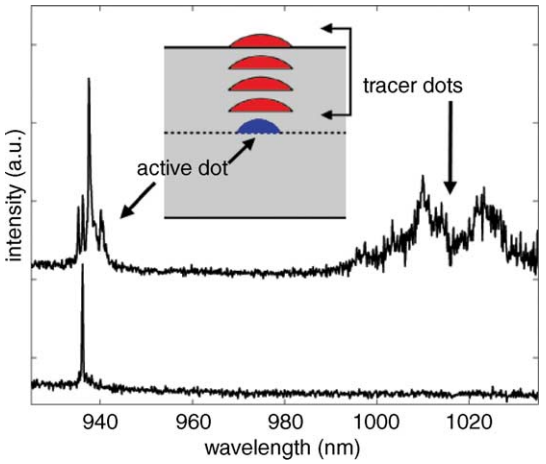

Fig. 4. Schematic of a stack of QDs in a photonic crystal slab layer used to position a cavity around a single dot in the middle of the slab. The stack consists of a seed QD with s-shell emission ~940 nm and a number of tracer dots with s-shells red-shifted beyond the detection range of our photo-detector. At low pump power, the stack behaves like a single exciton, while a 30 times increase in power reveals the excited states of the stack.

4. Positioning cavities to single quantum dots

The main obstacle to positioning a QD in a cavity is clear; it is difficult to know where the dot is with respect to some set coordinate system. This is a direct result of the restriction that the dot must be embedded vertically in the middle of the slab for both good coupling to the defect modes and to ensure the QD does not interact with surface states. We circumvent this problem by placing a mark, which we call a tracer, on the surface, directly above a viable QD that is buried 90 nm below. We can then use standard nanoscale metrological techniques to find this tracer and position a cavity around it. The tracer is formed during the epitaxy of the QD material by coherently stacking several QDs above a seed layer of QDs formed at the middle of the photonic crystal slab [17,18]. The resulting stack of QDs is shown schematically in the inset of Fig. 4. For an appropriate spacing between each layer of dots, the stacking occurs with very high probability, since the growing dots experience a strong nucleating force mediated by the strain field from the layer of dots beneath them. So that the tracer QDs do not interfere with optical experiments involving the exciton of the seed layer, we detune the exciton emission of the seed layer by over 150 nm to shorter wavelengths by growing them in an interrupted growth mode [19]. We will provide a detailed report on the material and optical properties of an individual stack (seed QD + tracer dots) in a separate publication. We present two spectra in Fig. 4 that show convincingly a single stack may be used as a single QD, even in the presence of the tracer dots. The lower spectrum is taken at a low pump power typically used for experiments involving a single exciton line. It is apparent that only the exciton of the seed QD is active at this power. If we increase the power by a factor of 30, the entire s-shell of the seed QD becomes active and we observe emission from the excited states of the stack, which are broad and very far detuned from the s-shell of the seed QD. It is clear that the tracer dots possess highly-red shifted energy levels that we expect will not interfere with the experiments on the exciton line of the seed QD at low pump power.

The tracer dot on the surface of the photonic crystal slab layer can be imaged using a SEM. However, since our JEOL electron-beam lithography system is not equipped to function as a high-resolution SEM, this prevents us from seeing the QDs with this tool and, hence, mapping the dots and writing the photonic crystal pattern in the same machine. Instead, we use an FEI Sirion field-emission SEM operating with a through-lens detector to generate detailed maps of several individual tracer dots relative to nearby Ti/

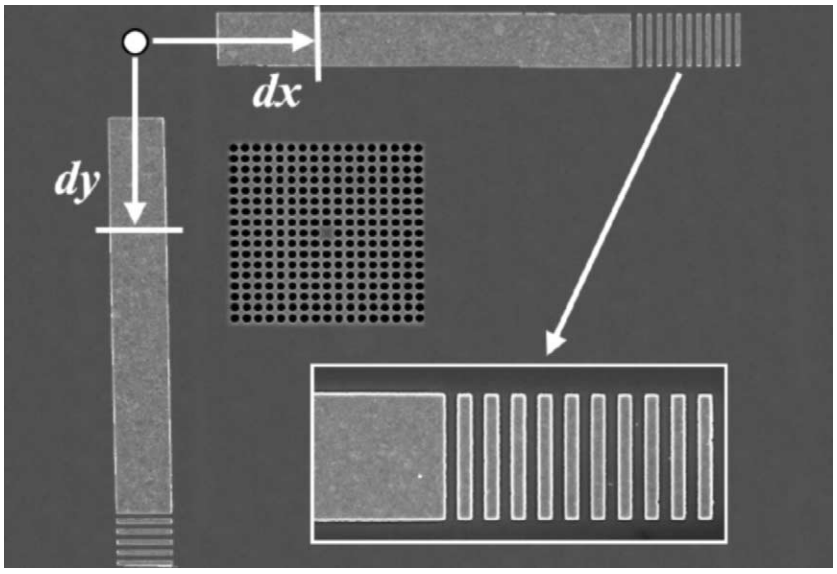

Fig. 5. Scanning electron micrograph of an optimized gold alignment mark used to position a single QD in a photonic crystal cavity. Precise alignment is only achieved if the arms of the mark have a constant width along their entire length and if the distance scale of the SEM used for mapping is scaled to the distance scale of the electron-beam lithography system using the calibration ruler shown in the inset. A cavity has been fabricated (d*x*,d*y*) from the origin of the mark.

Au (80/800 Å) alignment marks, deposited on the surface in an electron-beam lithography liftoff process. The goal of this mapping is to determine very precisely the distance in x and y between a tracer dot and the origin of the alignment mark. The type of alignment mark used is critical to achieve precise mapping. An SEM of a typical mark is shown in Fig. 5. A very important property of this alignment mark is that each arm has a constant width along its entire length. Our first alignment mark designs allowed the vertical and horizontal arms to intersect at the mark origin; however, due to the proximity effect introduced during the electron-beam lithography, the mark was overexposed at this intersection point, resulting in arms that were noticeably wider at the origin than far from it. This deviation in width was on the order of 50–100 nm and ultimately propagated to a final positioning error of the same order of magnitude. The present alignment marks avoid this overexposure and have a 2 μm width along their entire length, with a variation of ∼10 nm.

Since, the SEM mapping and the electron-beam lithography are performed in separate systems, it is critical to calibrate the distance scale of the SEM to that of the electron-beam lithography system. We observe a discrepancy of only 2% between the two systems' distance scales, yet this can result in a positioning error >100 nm if not corrected. A scale factor accounting for this difference is found by fabricating a "ruler" on the ends of both the vertical and horizontal arms of the alignment mark. This ruler is shown in the inset of Fig. 5 and has a periodicity of 400 nm as specified in the electron-beam lithography system. The scale factor is calculated by measuring the periodicity of the ruler in the SEM and dividing by 400 nm. Thus, any distance measurements made with the SEM can be easily translated into the electron-beam lithography system's coordinate frame for both the x and y directions, which may be different. We average the pitch of the ruler over the ten periods, reducing the effect of small errors introduced in the lift-off process. The error in the scale factor—and we estimate the final positioning error—is limited by the pixel size of the SEM image of the ruler, which is nominally 11 nm.

The final step of our active-positioning process is to detect the alignment marks in the electron-beam lithography system and write the cavity pattern a specified distance from the origin of the mark, corresponding to the scaled distances found during the SEM mapping. After transferring this pattern into the photonic crystal layer, the cavity is located a distance (dx, dy) from the

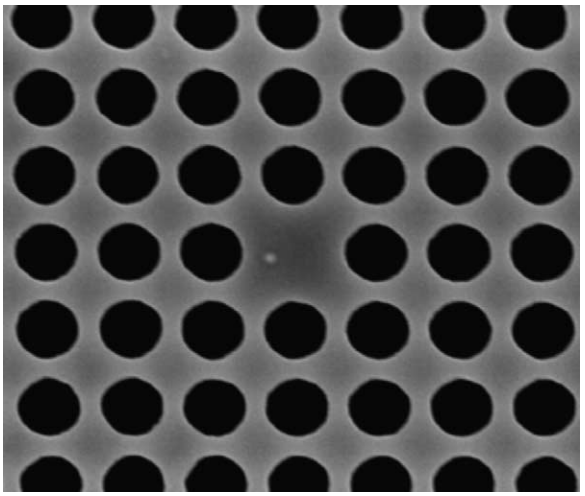

Fig. 6. Scanning electron micrograph showing the effectiveness of the active-positioning process. Here, a QD was intended to be positioned midway between the center of the defect and the first photonic crystal hole to the left of the defect, to coincide with a region of high field intensity. The positioning error is negligible.

origin of the mark as shown in Fig. 5, and we expect to find a QD positioned in the cavity. We have shown the effectiveness of this active positioning process by positioning several tracer dots in S1 cavities at the locations indicated by the white circles in Fig. 1. After fabrication of the cavities, we found that the tracer dot was positioned 20–25 nm from the target location for each device. Although we cannot generate a meaningful statistical analysis of this small $<1\%$ positioning error due to the prohibitive time needed to map in detail large numbers of QDs, we demonstrate an error no greater than 25 nm for every device fabricated according to the procedures explained in this report, convincing us of the repeatable accuracy of this process. We present Fig. 6 as an example of our active positioning process for a dot that was intended to be placed midway between the center of the defect and the first photonic crystal hole to the left of the defect. The SEM shows a negligible deviation from this target such that it is significantly overlapping a region of high electric field intensity shown in the field profile of Fig. 2. We have confirmed that after fabrication of the cavities, the seed QDs remain active and emit at nearly the same wavelength as before fabrication of the cavity. We are currently characterizing the interaction of the positioned seed QDs with the resonant modes of the cavities.

5. Conclusions

The active-positioning technique demonstrated in this work effectively solves one of the main obstacles to achieving reproducible coupling between a single QD and a defect cavity mode, namely placing the dot at a specific location within the cavity. The position of the QDs within the cavity can be specified with a resolution of 25 nm, which is adequate to spatially overlap an exciton captured in the QD with a region of high field intensity of the corresponding confined electromagnetic mode. This alignment has been achieved by coherently stacking tracer QDs above a seed QD up to the surface of the photonic crystal membrane layer, allowing us to ''see'' where the seed dot is simply by mapping the surface with an SEM. We have tested this alignment process by positioning several individual QDs in S1 photonic crystal cavities. This type of cavity supports a high Q/V whispering-gallery-like mode in a simple defect geometry that is relatively easy to fabricate, since every photonic crystal hole is specified to have the same diameter and spacing between adjacent holes. We have confirmed experimentally the high-Q/V of the WGM mode by measuring Q's as high as 8500. By carefully choosing a, r/a, and the electron dose deposited in the photonic crystal holes, we can match the WGM resonant wavelength to the exciton line of the mapped QDs to construct various devices for quantum information processing. This positioning technique is extremely useful for aligning to ultra-small V defect modes; however, in principle, it can be used to align single QDs to various other optical cavities or even electrically-addressing single-dot devices.

References

[1] A. Imamoglu, Physica E 16 (1) (2003) 47.
[2] O. Painter, J. Vuckovic, A. Scherer, J. Opt. Soc. Am. B 16 (2) (1999) 275.
[3] C. Reese, B. Gayral, B.D. Gerardot, A. Imamoglu, P.M. Petroff, E. Hu, J. Vac. Sci. Technol. B 19 (6) (2001) 2749.
[4] J. Vuckovic, M. Loncar, H. Mabuchi, A. Scherer, IEEE J. Quantum Electron. 38 (7) (2002) 850.
[5] K. Srinivasan, O. Painter, Opt. Express 10 (15) (2002).
[6] R. Han-Youl, H. Jeong-Ki, L. Yong-Hee, IEEE J. Quantum Electron. 39 (2) (2003) 314.
[7] Y. Akahane, T. Asano, B.S. Song, S. Noda, Nature 425 (2003) 944.

[8] P. Lalanne, J.P. Hugonin, IEEE J. Quantum Electron. 39 (11) (2003) 1430.
[9] T. Yoshie, J. Vuckovic, A. Scherer, C. Hao, D. Deppe, Appl. Phys. Lett. 79 (26) (2001) 4289.
[10] K. Srinivasan, P.E. Barclay, O. Painter, A.Y. Chen Jianxin, C. Cho, Gmachl, Appl. Phys. Lett. 83 (10) (2003) 1915.
[11] K. Hennessy, C. Reese, A. Badolato, C.F. Wang, A. Imamoglu, P.M. Petroff, E. Hu, G. Jin, S. Shi, D.W. Prather, Appl. Phys. Lett. 83 (18) (2003) 3650.
[12] K. Hennessy, C. Reese, A. Badolato, C.F. Wang, A. Imamoglu, P.M. Petroff, E. Hu, J. Vac. Sci. Technol. B 21 (6) (20032918).
[13] T. Yoshie, O.B. Shchekin, H. Chen, D.G. Deppe, A. Scherer, Electron. Lett. 38 (17) (2002) 967.
[14] Commercially available from Lumerical Solutions.
[15] C.F. Wang, A. Badolato, J. Urayama, I. Wilson-Rae, P.M. Petroff, A. Imamoglu, E. Hu, Appl. Phys. Lett., 2004, in press.
[16] K. Hennessy, C. Reese, A. Badolato, A. Imamoglu, P.M. Petroff, E.L. Hu, in: Proceedings of SPIE 5359, Soc. Opt. Eng., 2004, p. 210.
[17] A. Xie Qianghua, C. Madhukar, N.P. Ping, Kobayashi, Phys. Rev. Lett. 75 (13) (1995) 2542.
[18] G.S. Solomon, J.A. Trezza, A.F. Marshall, J.S. Harris Jr., Phys. Rev. Lett. 76 (6) (1996) 952.
[19] J.M. Garcia, T. Mankad, P.O. Holtz, P.J. Wellman, P.M. Petroff, Appl. Phys. Lett. 72 (24) (1998) 3172.